

The N II spectrum of the Orion Nebula

Vladimir Escalante¹ and Christophe Morisset² *

¹ *Centro de Radioastronomía y Astrofísica, Ap. Postal 72–3, C. P. 58091, Morelia, Michoacán, México*

² *Instituto de Astronomía, Ap. Postal 70–264, C. P. 04510, México, DF, México*

9 November 2018

ABSTRACT

The predicted emission spectrum of N II is compared with observations of permitted lines in the Orion nebula. Conventional nebular models show that the intensities of the more intense lines can be explained by fluorescence of starlight absorption with a N abundance that is consistent with forbidden lines. Lines excited mostly by recombination on the other hand predict high N abundances. The effects of stellar and nebular parameters and of the atomic data on the predicted intensities are examined.

Key words: line: formation— ISM: individual: Orion nebula

1 INTRODUCTION

Recent deep spectroscopic surveys of the Orion nebula (Esteban et al. 1998; Baldwin et al. 2000, hereafter BVV; Esteban et al. 2004, hereafter EPG) show that $N^{+2}+e$ recombination cannot explain the intensities of the N II permitted lines with a nitrogen abundance that is consistent with the N II forbidden line intensities. Seaton (1968) first suggested the possibility that permitted lines of C and O ions in nebulae may be excited by continuum fluorescence of starlight, and Grandi (1976) noted that this also must be an important mechanism to excite the N II lines in Orion. Grandi suggested that additional absorption of photons of the He I $1s^2\ ^1S_0-1s8p\ ^1P_1^\circ$ line at $\lambda 508.643\ \text{\AA}$ from the diffuse field of the nebulae by the N II $2p^2\ ^3P_0-2p4s\ ^3P_1^\circ$ transition at $\lambda 508.668\ \text{\AA}$ followed by decay to $3p$ terms would enhance the observed intensity of some lines. There is few direct evidence of the plausibility of this mechanism. BVV and EPG observed lines at $\lambda 3829.92$, $\lambda 3838.47$ and $\lambda 3856.27$ that could be produced by the $3p\ ^3P_1-4s\ ^3P_2^\circ$, $3p\ ^3P_2-4s\ ^3P_2^\circ$ and $3p\ ^3P_2-4s\ ^3P_1^\circ$ transitions respectively. Unfortunately those lines are probably blended with lines from other elements, and their identification and intensity are uncertain. Sharpee et al. (2003) have detected those and other lines of the $3p\ ^3P-4s\ ^3P^\circ$ multiplet in a planetary nebula (IC 418), where the N II spectrum is probably excited by fluorescence. The $4s\ ^3P_2^\circ$ level requires pumping of the the N II $2p^2\ ^3P_2-2p4s\ ^3P_2^\circ$ $\lambda 508.697\ \text{\AA}$ transition, which lies $32\ \text{km s}^{-1}$ from the He I line. Other lines from the $4s\ ^3P^\circ$ term like those of the $3p\ ^3D-4s\ ^3P^\circ$ multiplet in the $\lambda\lambda 3311.42-3331.31$ interval, which should be as intense as the $3p\ ^3P-4s\ ^3P^\circ$ multiplet, were not detected by EPG. The efficiency of this Bowen-type line fluorescence depends heavily on uncertain

nebular parameters that are needed in the theory of line radiative transfer, and modeling can become quite arbitrary. Therefore we will not consider it in this work (for further discussion see Escalante 2002; Liu et al. 2001).

The critical parameters that determine the intensities of the lines and the relative importance of the fluorescence mechanism over the recombination process are the N^+ and N^{+2} column densities in the gas and the stellar UV radiation field. Absorption of a UV photon by a resonant transition between a ground configuration state and an excited state has a higher probability of subsequent reemission in the same transition. Decay to an intermediate state will be favoured when the optical depth of the resonant transition is large, and the resonant photon is scattered a few times until it is converted into a lower energy photon producing a subordinate line. However the optical depth of the resonant transition must not become too large in order to allow enough resonant photons to penetrate into the N^+ zone. The efficiency of the continuum fluorescence excitation in N^+ depends on the transfer of resonant photons between the lowest resonant transition that can produce a subordinate line, $2p^2\ ^3P-3d\ ^3D^\circ$ $\lambda\lambda 533.51-533.88\ \text{\AA}$, and the ionization limit at $419\ \text{\AA}$. We have also included transitions from the $2p^2\ ^1D_2$ and 1S_0 metastable states—populated mostly by collisions—to other singlets in order to consider the observation of singlet lines in Orion. In the singlet system the lowest transition that produces a subordinate line is $2s^22p^2\ ^1S_0-2s2p^3\ ^1P_1^\circ$ $\lambda 745.84\ \text{\AA}$. Fig. 1 shows the observed transitions in Orion of the singlet and triplet N II systems. Possible observations of quintet lines and higher excitation states are discussed in section 4.4.

The observed intensities of permitted lines in planetary nebulae are often higher than their intensities predicted by recombination rates with CNO abundances measured from forbidden lines (Liu et al. 1995, 2001; Luo et al. 2001, and references therein). Some of the N II lines observed in PNe

* E-mail: v.escalante@astrosmo.unam.mx
morisset@astroscu.unam.mx

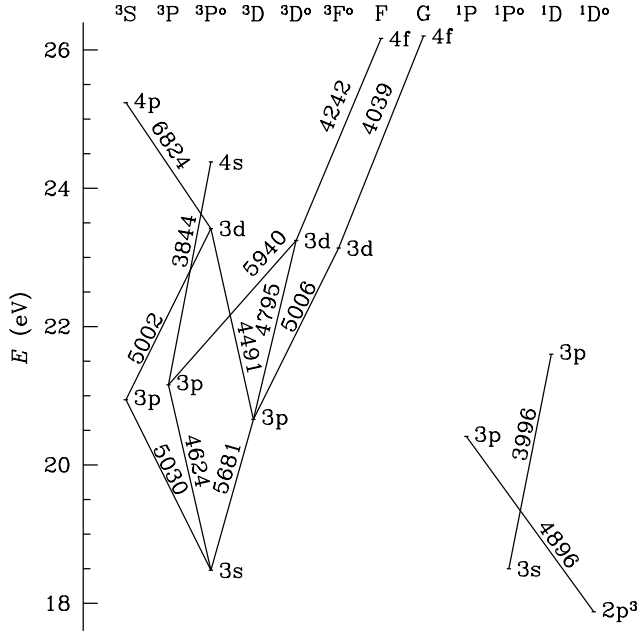


Figure 1. The singlet and triplet N II systems. Terms $3d\ ^3P^\circ$, $3d\ ^3D^\circ$ and $4s\ ^3P^\circ$ are connected by resonant transitions to the $2p^2\ ^3P$ ground term at 0 eV. Wavelengths are term-averaged values in Å.

have 4f upper levels, which are excited mainly by recombination. In Orion there exists a similar situation and we will show that fluorescence cannot account for the excess intensity of lines from 4f levels. The accuracy of the recombination theory can be more easily tested by comparing line ratios from 4f decays because all the transitions involved are optically thin and the absolute line intensities have a similar dependence on temperature and density.

The fluorescence theory is more difficult to test because it depends, often non-linearly, on several model parameters. We will use the ratio of predicted over observed intensities, averaged over all N II lines with reasonably accurate identifications and measurements, hereafter referred to as $R = \langle I_{\text{cal}}/I_{\text{obs}} \rangle$, to test the model parameters. The scatter around R will be used as a test of the atomic data and the details of the transferred stellar continuum.

Realistic nebular models and hot star model atmospheres along with available atomic data bases can explain successfully the intensities of a majority of the forbidden lines in Orion as well as general observed trends of ion abundances in Galactic H II regions (see for example Baldwin et al. 1991; Stasińska & Schaerer 1997). This paper demonstrates that the intensity of most of the N II permitted lines in the Orion nebula can be predicted by fluorescence of the starlight continuum and some contribution of recombination by these models with currently accepted physical conditions and abundances of the nebula.

2 CALCULATION OF POPULATION DENSITIES

2.1 Atomic processes

The important processes that can produce excited states with low principal quantum numbers in N^+ at nebular temperatures are absorption of UV photons by transitions from ground and metastable states and recombinations of N^{+2} . Subsequent decays of these states produce the optical N II spectrum. UV radiation is provided mostly by the star θ^1 C Ori. The contribution of the diffuse continuum to the absorption is negligible.

The number density of a N^+ excited state j at a certain point in the nebula in steady state, n_j , is given by

$$A_j n_j = \alpha_j n_e n(N^{+2}) + \sum_g \beta_{gj} n_g + \sum_{k>j} A_{kj} n_k, \quad (1)$$

where $A_j = \sum_i A_{ji}$ is the spontaneous decay rate, α_j is the recombination (radiative plus dielectronic) coefficient to state j , n_g is the population density of one of the five N^+ ground and metastable states, $2p^2\ ^3P_{0,1,2}$, $1D_2$, $1S_0$, and β_{gj} is the radiation absorption rate. If \bar{J}_ν is the local starlight mean intensity averaged over the absorption profile,

$$\beta_{gj} = \sigma_{gj} \left(\frac{4\pi \bar{J}_\nu}{h\nu} \right) \gamma_{gj}, \quad (2)$$

where $\sigma_{gj} = 0.02654 f_{gj} \text{ cm}^2 \text{ Hz}$ is the absorption cross section and f_{gj} is the f-value of transition $g \rightarrow j$. \bar{J}_ν is attenuated by continuum opacity and geometry. The “pumping probability” to account for the attenuation due to the transition $g \rightarrow j$ as defined by Ferland (1992) is

$$\gamma_{gj} = \int e^{-\tau_0 \phi(x)} \phi(x) dx, \quad (3)$$

where $\phi(x)$ is the normalized Voigt profile for a displacement $x = (\nu - \nu_0)/\Delta\nu$, and $\tau_0 = \sigma_{gj} N_g / \Delta\nu$ is the mean optical depth for a column density $N_g = \int n_g dr$ integrated along a ray from the star.

An actual stellar spectrum shows absorption lines superposed on the continuum and the P-Cygni profiles of the wind. If the structure of the stellar absorption spectrum varies in scales comparable to the width of $\Delta\lambda \sim 0.01 \text{ Å}$ of the UV resonant lines in the nebular gas, equation (3) should be changed to

$$\gamma_{gj} = \int \psi(x) e^{-\tau_0 \phi(x)} \phi(x) dx, \quad (4)$$

where $\psi(x) = J_\nu / \bar{J}_\nu$ is the continuum stellar profile around the resonant line. Grids with that resolution are available in the optical (Murphy & Meiksin 2004). In the UV Smith et al. (2002) and Sternberg et al. (2003) have published models with a lower resolution.

The populations of the metastable states at nebular temperatures are controlled by electron collisions, and are nearly independent of other excited states. The system of equations (1) is triangular, and can be solved in terms of the cascade matrix, C_{kj} (Seaton 1959). C_{kj} is the probability that a state j is produced by the excitation of state k followed by radiative decays by all possible routes ending in j . Equation (1) thus becomes

$$A_j n_j = \alpha_j^{\text{eff}} n_e n(N^{+2}) + \sum_g \beta_{gj}^{\text{eff}} n_g, \quad (5)$$

where

$$\alpha_j^{\text{eff}} = \sum_{k \geq j} \alpha_k C_{kj}, \quad (6)$$

$$\beta_{gj}^{\text{eff}} = \sum_{k \geq j} \beta_{gk} C_{kj}, \quad (7)$$

are the effective recombination coefficient and the effective fluorescence rate respectively. In practice the sums in equations (6) and (7) must be truncated and a correction must be added to equation (6) by extrapolation or by using hydrogenic populations (Escalante & Victor 1990, hereafter EV) because recombination coefficients of individual levels decrease slowly with n and the contribution of states with high angular momentum and high n must be included. Care must also be taken to avoid roundoff errors in the summations. The effective fluorescence rate in equation (7) is less sensitive to that type of correction because the absorption rate β_{gk} is non-zero only for states connected to the ground and metastable states by dipole-allowed transitions, and decreases more rapidly with the principal quantum number n of the upper state. The contribution of levels with $4 \leq n \leq 12$ and orbital angular momentum $0 \leq l \leq 2$ in equation (7) is less than 5% for the N II lines observed in Orion. The contribution of f states to the fluorescence rate is even less important because they are not connected by resonant transitions to the ground term, and the transitions $nd \rightarrow mf$ have a low relative probability. By eliminating states with $n > 9$ and $l > 2$ in equation (7), the CPU time decreases by a factor of 10. However the f states (and higher l states) must be included in the cascade due to recombinations, which tend to favor high-angular momentum states.

Most of the observed N II transitions in Orion come from decays of the 3p and 3d triplet terms. Practically all the excitations of the 3d terms are produced by direct absorptions in the multiplets $2s^2 2p^2 \ ^3P\text{--}2p3d \ ^3P^\circ \lambda\lambda 529.36\text{--}529.87 \text{ \AA}$ and $2s^2 2p^2 \ ^3P\text{--}2p3d \ ^3D^\circ \lambda\lambda 533.51\text{--}533.88 \text{ \AA}$. Cascades contribute negligibly to the populations of the 3d terms. The 3p terms, not being connected by direct transitions to the ground term, have more varied excitation channels. Between half and 80% of excitations of 3p terms come from decays of 3d terms. The rest comes mostly from absorptions in the multiplet $2s^2 2p^2 \ ^3P\text{--}2p4s \ ^3P^\circ \lambda\lambda 508.48\text{--}509.01 \text{ \AA}$ and higher s and d states. Table 1 shows a comparison of f -values for these multiplets, which are critical in our calculations.

The advantage of using the cascade matrix is that it needs to be computed once in the model in either the optically thin case (case A) or the extreme thick case (case B) because it depends solely on the Einstein coefficients, or more precisely, on the branching ratios $P_{kj} = A_{kj} / \sum_i A_{ki}$. In the escape probability formalism the equations must be modified by substituting the Einstein coefficients of transitions connected to the states of the ground configuration $2p^2 \ ^3P, \ ^1D, \ ^1S$ by $P_e A_{kg}$, where P_e is the escape probability to be discussed below. P_e is a local quantity that depends on the optical depth of the line as a function of position and thus the cascade matrix must be recomputed at each point in the nebula. However only a small fraction of the matrix elements depend on P_e . We found that recomputing only

Table 1. f absorption values for some N II resonant multiplets.

Multiplet	λ (Å)				
	(1)	(2)	(3)	(4)	(5)
$2p^2 \ ^3P\text{--}4s \ ^3P^\circ$	508.74	0.00987	0.0175	0.0105	0.0124
$2p^2 \ ^3P\text{--}3d \ ^3P^\circ$	529.68	0.102	0.175	0.103	0.138
$2p^2 \ ^3P\text{--}3d \ ^3D^\circ$	533.67	0.294	0.575	0.300	0.378

(1) Multiplet-averaged wavelength.

(2) Wiese et al. (1996).

(3) Victor & Escalante (1988).

(4) Seaton et al. (1994) (Opacity Project).

(5) Nussbaumer & Storey (1984).

this fraction of the cascade matrix reduces the CPU time by a factor of 30.

2.2 Escape probabilities

We have used the escape probability theory to handle nearly 200 resonant transitions that produce 2630 transitions by fluorescence. A review of the limitations of this theory has been given by Dumont et al. (2003), but a full line transfer calculation is beyond present computation capabilities. There are many approximations for the escape probability function, which differ by several factors at high optical depths. In an ionized nebula absorption of resonant photons by an overlapping continuum is important (Hummer 1968). In a uniform slab of total optical thickness T the escape probability at depth τ is $P_e = bF(b) + (1/2)[K_2(\tau, b) + K_2(T - \tau, b)]$, where the functions F and K_2 are defined in Hummer & Storey (1992), and $b = k_c/k_l$ is the continuum-to-mean line opacity ratio. The term

$$bF(b) = \int_0^\infty \frac{k_c}{k_l + k_c} \phi(x) dx, \quad (8)$$

is the probability that the resonant photon will be lost by continuum absorption. The effect of P_e is to increase considerably the probability that a resonant absorption decays into the subordinate line rather than reemitting the resonant photon. The average ratio, $R = \langle I_{\text{cal}}/I_{\text{obs}} \rangle$, increases by a factor of 20 between the two limits $P_e \equiv 1$ (case A) and $P_e \equiv 0$ (case B) respectively. A spectrum dominated by fluorescence, however, must be in an intermediate regime in order to allow the penetration of UV stellar photons through a large column density of absorbers at the same time that the resonant photons are scattered repeatedly.

All the resonant photons that produce the N II optical spectrum have a high probability of being lost by conversion into other lines besides being absorbed by the continuum, and the probability of a large number of scatterings is small. Consequently we used a Doppler core in the calculation of $K_2(\tau, b)$ and $F(b)$.

2.3 Atomic Data

The main source of A - and f -values for this work is the compilation of Wiese et al. (1996), which is based primarily on the Opacity Project data (Seaton et al. 1994) and

Table 2. Effective fluorescence rates for some N II lines.

Line	λ (Å)	$P_{ji} \sum_g \beta_{gj}^{\text{eff}} (10^{-8} \text{ s}^{-1})$			
i - j		(1)	(2)	(3)	(4)
3s $^3\text{P}_2^{\circ}$ –3p $^3\text{P}_2$	4630.5	10.8	25.7	16.1	13.7
3p $^3\text{D}_3$ –3d $^3\text{D}_3^{\circ}$	4803.3	4.6	4.5	4.5	4.6
3s $^3\text{P}_2^{\circ}$ –3p $^3\text{D}_3$	5679.6	7.1	16.3	10.3	8.9
3p $^3\text{P}_2$ –3d $^3\text{D}_3^{\circ}$	5941.7	8.0	8.6	8.6	8.0

(1) Only Wiese et al. (1996).

(2) Only Victor & Escalante (1988).

(3) Same as (2) plus doubly-excited configurations and $\Delta S \neq 0$ transitions.

(4) All transitions included.

configuration–interaction calculations, but also includes intermediate coupling calculations and experimental measurements. That compilation has data for most lines of the series $2s^2 2p(^2\text{P})nl$ with $n \leq 5$ and $l \leq 2$, and $2s2p(^4\text{P})nl$ with $n \leq 2$ and $l \leq 1$, including spin–forbidden transitions between quintet and triplet terms. The model potential calculations from Victor & Escalante (1988) were used for the rest of the transitions needed in the cascade matrix of the effective fluorescence rate in equation (7). Transition probabilities between fine structure levels were obtained by applying LS fractions to the multiplet data (Allen 1973).

Table 2 shows the effect of different atomic databases on the effective fluorescence rate (7) summed over the ground and metastable states times the branching ratio of the subordinate line. The continuum is a blackbody spectrum at $T = 37 \text{ kK}$ with a photon flux of $9.24 \times 10^{-4} \text{ cm}^{-2} \text{ s}^{-1} \text{ Hz}^{-1}$ at $\lambda 533.7 \text{ Å}$ and $\tau_0 = 0$ for all lines, i.e., $\gamma_{gj} = 1$, $P_e = 1$. The compilation of Wiese et al. (1996) does not include transitions to levels with principal quantum number greater than 5 and produce lower fluorescence rates of lines with upper p levels because those levels have cascade contributions from higher levels. The model potential data of Victor & Escalante (1988) does not have transitions to doubly-excited configurations and consequently give higher rates as shown in the fourth column of table 2. Transitions between states with the $2s2p^3$ configuration and the singly excited configurations $2s^2 2p3p$ can change the branching ratios significantly. The entries in the fifth column have been complemented with transitions to states with the $2s2p^2$ core configuration and spin-forbidden transitions taken from Wiese et al. (1996). The last column combines both data sets. The cascade matrix elements tend to be similar for different data sets because systematic differences in the atomic parameters between different data sets cancel out in the branching ratios $P_{ji} = A_{ji}/A_j$.

A recent calculation of effective recombination coefficients by Kisieliu & Storey (2002) shows a general agreement with the model potential calculations of Escalante & Victor (1990) (hereafter EV) and the calculations of Péquignot et al. (1991) for the $2s^2 2p(^2\text{P}^{\circ})3d$ and $4f$ configurations. The most important differences between the three calculations are in the branching ratios of multiplets from the $2s^2 2p(^2\text{P}^{\circ})3p \ ^3\text{D}$ term. The accuracy of the model potential in this case was limited by the lack of observed energies in the $2s^2 2p(^2\text{P}^{\circ})np$ series. The best agreement be-

tween the three data sets is in the $4f$ terms, where most of the contribution to the recombination comes from levels with small non-hydrogenic effects. The main uncertainty is in the line fractions involving $4f$ terms, where LS-coupling is not a good approximation. EV used LK coupling for these terms, and line fractions for other couplings are available (Escalante & Gongora 1990), but general intermediate-coupling calculations for those states are clearly needed.

This work uses the recombination coefficients of EV with branching ratios given by the A-values of Victor & Escalante (1988) and Wiese et al. (1996). Effective recombination coefficients for the levels of a term were obtained by assuming that the coefficients are proportional to the statistical weights of the levels.

3 MODEL CALCULATIONS

3.1 Nebular models

In order to determine the electron, N^{+2} , and N^{+} densities in equation (5), as well as the temperature and opacity at each point in the nebula, we used the codes CLOUDY (Ferland 1996, version 90.05) and NEBU (Péquignot et al. 2001; Morisset et al. 2002). Models of the Orion nebula support the existence of a main emitting layer at the back of a cavity in the OMC–1 molecular cloud. The thickness of the layer is highly variable across the nebula (Wen & O’Dell 1995). We approximated the layer by a plane–parallel model at constant pressure with CLOUDY and constant density with NEBU. CLOUDY allowed us to use the grain composition used by Baldwin et al. (1991) in their Orion model. Predicted line intensities by CLOUDY show some sensitivity when the radiation is included in the pressure law (Baldwin et al. 1996). Models with a constant gas pressure produce larger N^{+} column densities than models with a constant gas plus radiation pressure. We have not tried to find a single model fit to the observed forbidden line intensities in Orion. Instead we have run a series of models to find the most important dependencies of the N II lines excited by fluorescence on model parameters.

3.2 Model atmospheres

The Orion nebula is mostly excited by $\theta^1 \text{ C Ori}$. The other Trapezium stars increase the fluorescence of the N II lines by less than 2% and will not be considered in this calculation. $\theta^1 \text{ C Ori}$ is a class V star with variable wind features that produce uncertainties in the determination of its spectral classification and effective temperature. Different authors give values close to $T_{\text{eff}} = 39 \text{ kK}$ and $\log(g) = 4$ for this star (Howarth & Prinja 1989; Hillenbrand 1997, and references therein). However comparisons of the intensities of forbidden lines with nebular model predictions suggest temperatures as low as 36 kK (BVV). Metallicity measurements by Cunha & Lambert (1994) show that the Trapezium stars are slightly underabundant with respect to the Sun.

The calculation of the fluorescence of the gas needs a high resolution stellar spectrum. This is important with hot massive stars, which have expanding atmospheres with a dense forest of absorption lines and broad overlapping P Cygni profiles. The emission peaks and absorption troughs of

Table 3. Model parameters for the basic model (BM)

T_{eff}^*	37 kK	n	10^4 cm^{-3}
$\log g$	4.0	He	0.095
Z	$1Z_{\odot}$	C	3×10^{-4}
ϕ_0^*	$10^{12.9} \text{ s}^{-1} \text{ N}^*$		6×10^{-5}
θ	0°	O	4×10^{-4}
$V_{\text{turbulent}}$	8 km s^{-1}	Ne	6×10^{-5}

* Variable parameters in this work.

the overlapping P Cygni profiles can increase or decrease the absorption rate in equation (3) by large factors and change the fluorescence excitation rate significantly. On the other hand nebular models usually smooth the spectrum of the exciting star to calculate the ionization structure. In order to take into account the detailed spectral structure of the model atmosphere, we input the unattenuated stellar spectrum into the nebular model and extracted the predicted attenuated local continuum at each point in the nebula. To calculate the pumping rate in equation (3), the full resolution spectrum was read and interpolated at the absorption frequency and was scaled by the ratio of the attenuated to the unattenuated stellar continuum predicted by the nebular model.

The motion of the star with respect to the gas introduces a Doppler shift that can change the intensity of the continuum at the absorbing frequencies. The proper motion velocity of θ^1 C Ori is uncertain (Wen & O'Dell 1995). Doppler shifts of up to $\pm 30 \text{ km s}^{-1}$ did not change predicted line intensities by more than a few percent with the resolution of about $\Delta\lambda \sim 1 \text{ \AA}$ in the far UV of the model atmospheres that we used. Therefore we assumed a static star with respect to the gas.

Recent model atmospheres of O stars include the effects of line blanketing and line blocking of the stellar wind. We used model atmospheres calculated with the WMBASIC code (Pauldrach et al. 2001; Sternberg et al. 2003) to account for these effects. We also used the LTE, line-blanketed atmospheres of Kurucz (1991) for comparison purposes.

4 BASIC MODEL

All transitions of the observed permitted lines in Orion end in excited states and are optically thin. Their intensities can thus be obtained by integration of the emissivity along the line of sight:

$$I = \frac{h\nu}{4\pi} \int A_{ji} n_j dr \quad (9)$$

We now examine the dependence of the fluorescence excitation on the stellar spectrum and the density and compare them with the observations of BVV and EPG.

We have adopted a set of central values for the parameters of the models that are given in table 3. These values are close to the ones recommended by Baldwin et al. (1991), and we will refer to them as the basic model (BM). We discuss below a few features of this model.

4.1 Gas abundances and density.

The N^{+2} abundance in the nebula can be estimated from the measurements of lines with upper 4f levels, which are populated mostly by recombination. Table 4 lists the observed intensities of these lines in Orion and their predicted recombination emission rates normalized to the observed intensities and recombination rate of the $3s \text{ } ^3\text{P}_2^o - 3p \text{ } ^3\text{D}_3 \lambda 5679.56 \text{ \AA}$ line. BVV and EPG measured the lines at $\lambda\lambda 4236.91, 4237.05$ and 4241.784 , which account for 92% of the total strength of the $3d \text{ } ^3\text{D}^o - 4f \text{ F}$ multiplet if the 4f levels are described by an LK coupling scheme as shown in the table. We do not include in the abundance estimation the $\lambda 4242.49$ line because its measured intensity is much higher than the one predicted from the recombination theory. At $T_e = 10^4 \text{ K}$ the effective recombination coefficient of multiplet $3d \text{ } ^3\text{D}^o - 4f \text{ F}$ is $5.6 \times 10^{-14} \text{ cm}^3 \text{ s}^{-1} \text{ (EV)}$, which implies $\text{N}^{+2}/\text{H}^+ = 9.5 \times 10^{-5}$ if the lines were produced solely by recombination. This abundance is higher than the one implied by the forbidden lines $\approx 6 \times 10^{-5}$ in Orion and many galactic H II regions (e.g., Shaver et al. 1983; Aflerbach et al. 1977).

We notice that EPG detected one line from the $3d \text{ } ^3\text{F}^o - 4f \text{ G}$ multiplet ($\lambda 4041.31$) although other lines of this multiplet theoretically should be more intense than the observed lines of the $3d \text{ } ^3\text{D}^o - 4f \text{ F}$ multiplet. The corresponding N^{+2}/H^+ abundance from this line is 8.5×10^{-5} . Liu et al. (2001) has reported a N^{+2} abundance of 4.47×10^{-5} in Orion from the $\lambda\lambda 4041.31$ and 4043.53 lines, which is more consistent with the abundance from the forbidden lines.

Several authors (Liu et al. 2000, 2001; Tsamis et al. 2003; Peimbert et al. 2004) have detected N II lines in planetary nebula with relative rates that are more compatible with the recombination theory and will be the subject of future work. In a typical H II region there is not enough N^{+2} column density to produce a N^+ recombination spectrum. Fig. 2 shows separately the intensities given by equation (9) (integrated from right to left) due to recombination and fluorescence as a function of depth for a line. While the recombination intensity grows linearly with distance the fluorescence intensity grows more rapidly. The fluorescence excitation is favoured by the more intense starlight continuum and low opacity in the near side of the nebula, while the recombination emissivity is more uniformly distributed. In the far side of the nebula the high optical depth in a resonant line scatters more photons and increases the probability of re-absorption in the line, thus increasing the pumping of the fluorescence emission. The measurements by BVV show that most N II permitted lines are blueshifted by 2 or 3 km s^{-1} with respect to the N II forbidden lines, and support the idea that they are formed in different layers of the nebula.

We have chosen as a starting point the set of gas abundances of Baldwin et al. (1996), which were derived to fit forbidden line intensities with CLOUDY. The only exception was nitrogen for which we took a value of 6×10^{-5} as an average from the determinations of Baldwin et al. (1996) and EPG. Differences in the abundances of the other elements between the two sets are not important in N II permitted line intensities.

The N^+ column density remains remarkably constant with varying gas density for a given effective temperature of the star, T_{eff} . For the $T_{\text{eff}} = 37 \text{ kK}$, $\log g = 4$ atmosphere, $\text{N}(\text{N}^+) = 2.5 \times 10^{16} \text{ cm}^{-2}$ for gas densities between 4,000

Table 4. Intensities of lines from 4f levels in Orion and PNe [$I(\text{N II } \lambda 5679.56) = 1$].

LK Multiplet	Line	λ (Å)	%	Theory	Orion		PNe		
3d $^3\text{L}_J^\circ$ –4f L'[K] $_{J'}$	J–[K] $_{J'}$	J–[K] $_{J'}$	(1)	(2)	(3)	(4)	(5)	(6)	(7)
3d $^3\text{F}_J^\circ$ –4f G[K] $_{J'}$	3–[9/2]4	4026.08	13.9	0.24	*	*	*	*	*
	2–[7/2]3	4035.08	23.8	0.41	–	–	0.24	0.23	0.32
	4–[9/2]5	4041.31	40.7	0.70	–	0.30	0.58	0.53	0.58
	3–[7/2]4	4043.53	17.4	0.30	–	–	0.35	0.21	0.23
3d $^3\text{D}_J^\circ$ –4f G[K] $_{J'}$	3–[7/2]3	4201.35	–	–	–	0.14	–	–	–
3d $^3\text{D}_J^\circ$ –4f F[K] $_{J'}$	1–[5/2]2	4236.93	20.0	0.20	0.23	0.16	{ 0.17 0.26 }	0.13 0.20	0.16 0.23
	2–[7/2]3	4237.05	12.7	0.13					
	2–[5/2]2	4241.24	3.7	0.04	–	–	0.04	0.04	0.04
	2–[5/2]3	4241.76	16.9	0.17	0.20	0.28	0.49	0.54	0.51
	3–[7/2]4	4241.79	42.9	0.42					
	3–[7/2]3	4242.49	1.6	0.02	–	0.28	–	–	–

* Blended with He I.

(1) Line fraction in LK coupling.

(2) Calculated from recombination rates at $T = 10^4$ K in case A, EV.

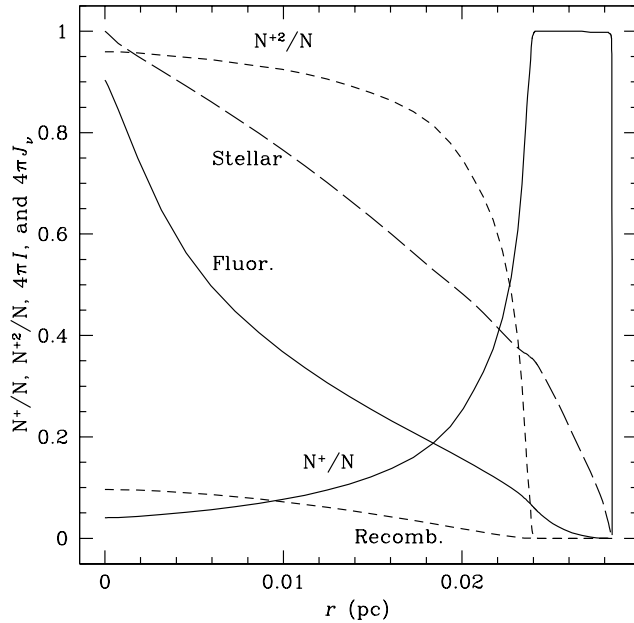
(3) BVV.

(4) EPG.

(5) NGC 6153, Liu et al. (2000), intensities from scanned spectrum.

(6) M 1–42, Liu et al. (2001).

(7) M 2–36, Liu et al. (2001).

**Figure 2.** Ion fractions of N^+ , N^{+2} , fluorescence and recombination contribution to the intensity of the 5941.65 Å line and stellar continuum (long dash) at 533.73 Å as functions of geometrical depth in parsecs. The intensities are normalized to the total intensity of the line, $4\pi I = 5.14 \times 10^{-4} \text{ erg cm}^{-2} \text{ s}^{-1}$ and to the stellar flux on the illuminated side of the nebula, $4\pi \bar{J}_\nu = 1.402 \times 10^{-3} \text{ erg cm}^{-2} \text{ s}^{-1} \text{ Hz}^{-1}$. Earth and $\theta^1 \text{ C Ori}$ are to the left.

and $25,000 \text{ cm}^{-3}$. Therefore we will adopt a fixed density of $n = 10^4 \text{ cm}^{-3}$.

4.2 Stellar continuum and geometry

The blister model, in which $\theta^1 \text{ C Ori}$ is near the wall of the OMC–1 molecular cloud (Zuckerman 1973; Balick et al. 1974), gives the most likely geometry for the nebula. The Lyman photon flux of the star at a distance r_0 from the illuminated face of the nebula is $\phi_0 = Q_0/4\pi r_0^2$, and can be constrained by the $\text{H}\beta$ observed brightness up to a geometrical factor that depends on the angle of illumination θ of the slab of gas as described by Wen & O’Dell (1995). The value $\phi = 10^{12.9} \text{ cm}^{-2} \text{ s}^{-1}$ and $\theta = 0$, fixes the $\text{H}\beta$ intensity around $4\pi I = 2.6 \text{ erg cm}^{-2} \text{ s}^{-1}$ observed by Baldwin et al. (1991) if corrections are considered to account for reflected optical and absorbed UV radiations (Ferland 2001). The $T_{\text{eff}} = 37 \text{ kK}$ is too low for the probable spectral type of $\theta^1 \text{ C Ori}$, but was chosen because it reproduces the absolute intensities of the fluorescence lines with respect to the $\text{H}\beta$ flux and the N abundance measured from forbidden lines as discussed in section 5.1.

4.3 The recombination spectrum.

The 4f levels in N^+ are in an intermediate coupling between LK and jK couplings (Cowan & Andrew 1965). In both couplings the total angular momentum is $J = K \pm 1/2$. The line fractions for either coupling can be obtained from Escalante & Gongora (1990). We employed an LK classification to use the recombination rates of EV.

Table 4 shows that all but two of the observed ratios of intensities of lines from 4f levels with respect to lines from 3d levels tend to be twice as strong and are closer to their predicted values by the recombination theory in PNe than in Orion. The two exceptions are the $\lambda 4242.49$ line, which seems much stronger than its predicted recombination rate, and the line of the 3d $^3\text{D}^\circ$ –4f G[7/2] multiplet, which violates the $\Delta L = 0, \pm 1$ selection rule in LK coupling due to strong mixing with the 4f F[7/2] term (Cowan & Andrew 1965), and has no predicted recombination rate by EV.

Liu et al. (2000, 2001) observed lines from other 4f terms in PNe, which have not been detected in Orion and are not listed in table 4. The higher intensity of the lines from 4f levels with respect to the lines from 3d levels in PNe indicates that fluorescence is less important relative to recombination in these objects because recombination can efficiently populate levels with high angular momentum while fluorescence is limited to resonant levels. One important exception to this trend is PN IC 418, which shows a strong enhancement of lines from 3p and 3d levels with respect to lines from the 4f levels (Sharpee et al. 2003). This nebula has a lower ionization level than most PNe that favors the excitation of N II lines by fluorescence over recombination as in Orion, and will be the subject of a forthcoming paper.

Fluorescence can only contribute to population of the 4f levels through transitions from higher d levels, but this process is inefficient because the transition probabilities are much smaller than transitions to p levels. For example, fluorescence can populate the 4f F levels through absorptions in the multiplet $2p^2\ ^3P\text{--}5d\ ^3D^\circ\lambda 453$, but in a pure case B the $5d\ ^3D^\circ$ term decays to the terms $3p\ ^3P$, $3p\ ^3D$, $2s2p^2(^4P)3s\ ^3P$, $4p\ ^3P$ and $4f\ F$ among others with branching ratios $P(5d, 3p\ ^3P) = 0.70$, $P(5d, 3p\ ^3D) = 0.14$, $P(5d, 3s) = 0.09$, and $P(5d, 4f) = 0.04$. As shown in section 4.1, N^{+2} abundances obtained from recombination rates of the 4f lines in Orion are 1.6 times the N abundance derived from collisionally excited lines. Suppose that the intensity of a 3d–4f line were enhanced with respect to $H\beta$ by fluorescence populating the 5d term with rate $B(5d)$:

$$\frac{I_\lambda}{I_{H\beta}} = \frac{4861}{\lambda} P(\lambda) \frac{E + P(5d, 4f)B(5d)}{E(H\beta)} \quad (10)$$

where $E(H\beta) = \int \alpha_{H\beta}^{\text{eff}} n(H^+) n_e d\ell$, $E = \int \alpha_{4fF}^{\text{eff}} n(N^{+2}) n_e d\ell$ and $P(\lambda)$ is the branching ratio of the 3d–4f line with λ given in Å. To account for the excess abundance of 0.6 obtained from the effective recombination rate of multiplet $3d\ ^3D^\circ\text{--}4f\ F\lambda\lambda 4236.91\text{--}4247.20$, we need $B(5d) = 0.6E/P(5d, 4f)$, which means a rate of population of the $3p\ ^3P$ term of $B(5d)P(5d, 3p\ ^3P) = 10.5E$. The contribution to the intensity of a multiplet like $3s\ ^3P\text{--}3p\ ^3P\lambda\lambda 4601.48\text{--}4643.08$ due to this additional excitation with $N^{+2}/H^+ \approx 6 \times 10^{-5}$ would be $B(5d)P(5d, 3p\ ^3P)P(3p\ ^3P, 3s\ ^3P^\circ)/E(H\beta) = 7.7 \times 10^{-4}$ where we took $P(3p\ ^3P, 3s\ ^3P^\circ) = 0.36$ and an effective recombination coefficient of the 4f F term $\alpha_{4fF}^{\text{eff}} = 1.0 \times 10^{-13} \text{ cm}^3 \text{ s}^{-1}$ at 10^4 K (EV). The strongest line of the multiplet, $3s\ ^3P_2^\circ\text{--}3p\ ^3P_2\lambda 4630.54$, has an LS line fraction of 11.25/27 (Allen 1973) and the corresponding increase in intensity would be at least 0.034 ($I(H\beta) = 100$), which is comparable the observed intensity of 0.048 (EPG) produced by more direct cascade routes following absorption of photons at $\lambda\lambda 530$ and 534 Å by 3d states. Thus the excitation of 4f states by fluorescence would produce lines from 3p and 3d states with intensities much higher than the observed values unless the stellar continuum had an unusual shape that selectively excited states above the 4f states. Our calculations show negligible contribution of fluorescence to the excitation of the 4f levels because the absorption rate is much less for higher resonant levels than for the 3d levels, and point to other mechanisms to excite them (Tsamis et al. 2004).

EPG also observed the lines at $\lambda 5001.14$ and 5001.48 with upper levels $3d\ ^3F_{2,3}^\circ$. The most intense component

of the multiplet at $\lambda 5005.15$ is blended with the $[O\text{ III}]\lambda 5005.15$ line. As with the lines with upper 4f levels, the $\lambda 5005.15$ line is mostly excited by recombination because its upper level $3d\ ^3F_4^\circ$ can receive only indirect contributions from the fluorescence excitation of higher levels. The other levels, $3d\ ^3F_{2,3}^\circ$, are connected to the ground state through weak dipole-allowed transitions (Bell et al. 1995), and have a substantial fluorescence contribution. Our model calculations show that fluorescence contributes less than 5% to the intensity of the lines produced by the $3d\ ^3F_4^\circ$ and 4f levels in Orion, and it is not sufficient to explain the discrepancy between the abundances determined from recombination and collisionally excited lines.

4.4 The fluorescence spectrum

Table 5 gives the predicted intensities for the observed upper terms in Orion by BVV and EPG that are excited mostly by fluorescence. Although the two data sets are from different parts of the nebula, it is important to notice that both sets give similar measurements of the N II permitted line intensities with respect to $H\beta$. Uncertain observed intensities due to blends, low S/N or dubious identifications are marked with “?” in the table as indicated by those authors. We also added a question mark to the line at 4987.4 Å , which is probably blended with the $[\text{Fe III}]\lambda 4987.20$ line, and thus has an observed intensity much higher than our prediction. The line at 4994.4 Å belonging to the same multiplet should be theoretically more intense, contrary to the observations.

The most intense fluorescence lines are triplets connected by resonant transitions to the ground term, $2p^2\ ^3P$. At temperatures characteristic of H II regions, the fine structure populations of the ground term are approximately proportional to their statistical weight, and consequently the relative intensities of all the other triplet levels are given by the LS line fractions (Allen 1973).

The lines at 5001.15 and 5001.48 Å arising from the $3d\ ^3F^\circ$ term are blended. We split the total intensity according to the LS line fractions: 21.0:31.1, in order to compare them with our predictions in table 5.

Multiplet $3p\ ^3P\text{--}4s\ ^3P^\circ$ has many strong lines in the $\lambda 3838.37\text{--}3856.06 \text{ Å}$ interval that were not detected because of the lower S/N at the blue end of the spectrum and because they are blended with other lines. Therefore they are not listed in table 5.

EPG marginally detected the $3d\ ^3P_2^\circ\text{--}4p\ ^3S_1\lambda 6809.99 \text{ Å}$ line. Lines from the 4p levels must be excited by cascades from upper levels in a fluorescence spectrum. We found very low intensities for all the lines from 4p levels. The most intense line of this type is $2p^3\ ^3P_2^\circ\text{--}4p\ ^3S_1\lambda 1060.2 \text{ Å}$ with an intensity of 4×10^{-5} with respect to $H\beta$. Our predicted intensities of lines from 4p levels in the optical are below the instrumental sensitivity.

In table 5 we also list some singlets because BVV marginally detected the $2p^3\ ^1D_2^\circ\text{--}3p\ ^1P_1\lambda 4895.11 \text{ Å}$ line. Singlets can be excited by absorptions from the 1D and 1S terms of the ground configuration, spin-forbidden transitions from the triplets and recombination. The quintet lines $3p\ ^5D_1^\circ\text{--}3d\ ^5P_1\lambda 4815.62 \text{ Å}$, $3s\ ^5P_{1,3}\text{--}3p\ ^5D_{1,4}\lambda 5535.36 \text{ Å}$ and $3s\ ^5P_3\text{--}3p\ ^5D_3\lambda 5551.99 \text{ Å}$ measured by BVV and EPG are not listed. These lines have the $2s2p^2\ ^4P$ excited core configuration, and can only be populated with transitions in

Table 5. Predicted intensities of the basic model (BM) and observations ($I(\text{H}\beta) = 10^4$) for lines excited by fluorescence. The nebular model was calculated with CLOUDY.

Transition	λ (Å)	I_r/I (1)	$I/I(\text{H}\beta)$ (2)	$I/I(\text{H}\beta)$ (3)	$I/I(\text{H}\beta)$ (4)
$2p^3 \ ^3P_0^o-4p \ ^3S_1$	1060.2	0.362	0.38	–	–
$2p^3 \ ^3P_1^o-4p \ ^3S_1$	1060.2	0.362	0.37	–	–
$2p^3 \ ^3P_0^o-4p \ ^3S_1$	1060.3	0.362	0.15	–	–
$2p^3 \ ^3D_3^o-3p \ ^3P_2$	1275.0	0.118	17.31	–	–
$2p^3 \ ^3D_2^o-3p \ ^3P_2$	1275.3	0.118	3.15	–	–
$2p^3 \ ^3D_1^o-3p \ ^3P_2$	1275.3	0.118	0.21	–	–
$2p^3 \ ^3D_1^o-3p \ ^3P_1$	1276.2	0.094	3.92	–	–
$2p^3 \ ^3D_2^o-3p \ ^3P_1$	1276.2	0.094	11.62	–	–
$2p^3 \ ^3D_1^o-3p \ ^3P_0$	1276.8	0.079	6.01	–	–
$2p^3 \ ^3D_3^o-3p \ ^3D_3$	1343.3	0.257	3.30	–	–
$2p^3 \ ^3D_2^o-3p \ ^3D_3$	1343.6	0.257	0.39	–	–
$2p^3 \ ^3D_3^o-3p \ ^3D_2$	1345.1	0.176	0.68	–	–
$2p^3 \ ^3D_1^o-3p \ ^3D_2$	1345.3	0.176	0.55	–	–
$2p^3 \ ^3D_2^o-3p \ ^3D_2$	1345.3	0.176	2.63	–	–
$2p^3 \ ^3D_1^o-3p \ ^3D_1$	1346.4	0.167	1.80	–	–
$2p^3 \ ^3D_2^o-3p \ ^3D_1$	1346.4	0.167	0.66	–	–
$2p^3 \ ^3P_1^o-3p \ ^3P_2$	1627.3	0.118	0.13	–	–
$2p^3 \ ^3P_2^o-3p \ ^3P_2$	1627.4	0.118	0.46	–	–
$2p^3 \ ^3P_2^o-3p \ ^3P_1$	1628.9	0.094	0.30	–	–
$2p^3 \ ^3P_1^o-3p \ ^3P_1$	1628.9	0.094	0.07	–	–
$2p^3 \ ^3P_0^o-3p \ ^3P_1$	1629.1	0.094	0.11	–	–
$2p^3 \ ^3P_1^o-3p \ ^3P_0$	1629.8	0.079	0.18	–	–
$2p^3 \ ^3P_1^o-3p \ ^3S_1$	1675.7	0.084	5.43	–	–
$2p^3 \ ^3P_2^o-3p \ ^3S_1$	1675.8	0.084	8.87	–	–
$2p^3 \ ^3P_0^o-3p \ ^3S_1$	1675.9	0.084	1.83	–	–
$2p^3 \ ^3P_2^o-3p \ ^3D_3$	1740.3	0.257	9.39	–	–
$2p^3 \ ^3P_2^o-3p \ ^3D_2$	1743.2	0.176	2.39	–	–
$2p^3 \ ^3P_1^o-3p \ ^3D_2$	1743.2	0.176	7.32	–	–
$2p^3 \ ^3P_1^o-3p \ ^3D_1$	1745.0	0.167	2.54	–	–
$2p^3 \ ^3P_2^o-3p \ ^3D_1$	1745.1	0.167	0.17	–	–
$2p^3 \ ^3P_0^o-3p \ ^3D_1$	1745.3	0.167	3.45	–	–
$3s \ ^3P_0^o-4p \ ^3S_1$	1830.5	0.362	0.01	–	–
$3s \ ^3P_1^o-4p \ ^3S_1$	1831.6	0.362	0.02	–	–
$3s \ ^3P_2^o-4p \ ^3S_1$	1836.2	0.362	0.06	–	–
$2p^3 \ ^1D_2^o-3p \ ^1D_2$	3329.7	0.454	0.01	–	–
$3s \ ^3P_1^o-3p \ ^1D_2$	3955.8	0.454	0.06	–	–
$3s \ ^1P_1^o-3p \ ^1D_2$	3995.0	0.454	0.60	–	1.0?
$3p \ ^1P_1-3d \ ^3P_1^o$	4114.3	0.014	0.01	–	–
$3p \ ^1P_1-3d \ ^3D_2^o$	4375.0	0.035	0.03	–	–
$3p \ ^1P_1-3d \ ^3D_1^o$	4379.6	0.016	0.01	–	–
$3p \ ^3D_1-3d \ ^3P_0^o$	4459.9	0.014	0.15	–	–
$3p \ ^3D_1-3d \ ^3P_1^o$	4465.5	0.014	0.09	1.5?	–
$3p \ ^3D_2-3d \ ^3P_1^o$	4477.7	0.014	0.34	–	–
$3p \ ^3D_2-3d \ ^3P_2^o$	4488.1	0.033	0.06	–	–
$3p \ ^3D_3-3d \ ^3P_2^o$	4507.6	0.033	0.45	–	–
$3p \ ^1P_1-3d \ ^3F_2^o$	4564.8	0.467	0.02	–	–
$3s \ ^3P_1^o-3p \ ^3P_2$	4601.5	0.118	2.01	1.5	1.3
$3s \ ^3P_0^o-3p \ ^3P_1$	4607.2	0.094	2.11	5.7?	4.2
$3s \ ^3P_1^o-3p \ ^3P_1$	4613.9	0.094	1.46	0.9?	1.0
$3s \ ^3P_1^o-3p \ ^3P_0$	4621.4	0.079	2.38	1.8?	1.6
$3s \ ^3P_2^o-3p \ ^3P_2$	4630.5	0.118	6.57	4.6	4.8
$3s \ ^3P_2^o-3p \ ^3P_1$	4643.1	0.094	2.89	2.2	1.5
$3s \ ^1P_1^o-3p \ ^3P_2$	4654.5	0.118	0.21	–	–
$3s \ ^1P_1^o-3p \ ^3P_1$	4667.2	0.094	0.19	–	–
$3s \ ^1P_1^o-3p \ ^3P_0$	4674.9	0.079	0.26	–	–

Table 5 – continued

Transition	λ (Å)	I_r/I (1)	$I/I(\text{H}\beta)$ (2)	$I/I(\text{H}\beta)$ (3)	$I/I(\text{H}\beta)$ (4)
$3p \ ^3D_1-3d \ ^3D_2^o$	4774.2	0.035	0.16	–	–
$3p \ ^3D_1-3d \ ^3D_1^o$	4779.7	0.016	1.11	0.8	1.1
$3p \ ^3D_2-3d \ ^3D_3^o$	4781.2	0.096	0.09	–	–
$3p \ ^3D_2-3d \ ^3D_2^o$	4788.1	0.035	1.26	1.2	1.4
$3p \ ^3D_2-3d \ ^3D_1^o$	4793.6	0.016	0.34	1.1?	–
$3p \ ^3D_3-3d \ ^3D_3^o$	4803.3	0.096	1.45	1.3	1.9
$3p \ ^3D_3-3d \ ^3D_2^o$	4810.3	0.035	0.24	–	–
$2p^3 \ ^1D_2^o-3p \ ^1P_1$	4895.1	0.231	0.07	1.7?	–
$3p \ ^3S_1-3d \ ^3P_0^o$	4987.4	0.014	0.89	7.6?	4.6?
$3p \ ^3S_1-3d \ ^3P_1^o$	4994.4	0.014	2.65	1.3?	1.8
$3p \ ^3D_1-3d \ ^3F_2^o$	5001.1	0.467	1.10	–	1.2
$3p \ ^3D_2-3d \ ^3F_3^o$	5001.5	0.375	2.30	–	1.8
$3s \ ^3P_0^o-3p \ ^3S_1$	5002.7	0.084	0.53	–	–
$3p \ ^3D_3-3d \ ^3F_4^o$	5005.2	0.944	1.44	–	–
$3p \ ^3S_1-3d \ ^3P_2^o$	5007.3	0.033	3.23	–	–
$3s \ ^3P_1^o-3p \ ^3S_1$	5010.6	0.084	1.38	–	–
$3p \ ^3D_2-3d \ ^3F_2^o$	5016.4	0.467	0.18	–	–
$3p \ ^3D_3-3d \ ^3F_3^o$	5025.7	0.375	0.23	–	–
$3s \ ^3P_2^o-3p \ ^3S_1$	5045.1	0.084	2.13	–	1.4
$3s \ ^1P_1^o-3p \ ^3S_1$	5073.6	0.084	0.16	–	–
$3p \ ^3S_1-3d \ ^3D_2^o$	5383.7	0.035	0.01	–	–
$3p \ ^3S_1-3d \ ^3D_1^o$	5390.7	0.016	0.01	–	–
$3p \ ^3P_0-3d \ ^3P_1^o$	5452.1	0.014	0.28	–	–
$3p \ ^3P_1-3d \ ^3P_0^o$	5454.2	0.014	0.36	–	–
$3p \ ^3P_1-3d \ ^3P_1^o$	5462.6	0.014	0.32	–	–
$3p \ ^3P_1-3d \ ^3P_2^o$	5478.1	0.033	0.18	–	–
$3p \ ^3P_2-3d \ ^3P_1^o$	5480.1	0.014	0.41	–	–
$3p \ ^3P_2-3d \ ^3P_2^o$	5495.7	0.033	0.89	0.7	0.5?
$3s \ ^3P_1^o-3p \ ^3D_2$	5666.6	0.176	4.63	3.1	2.9
$3s \ ^3P_0^o-3p \ ^3D_1$	5676.0	0.167	2.32	1.2	1.0?
$3s \ ^3P_2^o-3p \ ^3D_3$	5679.6	0.257	6.24	4.3	4.3
$3s \ ^3P_1^o-3p \ ^3D_1$	5686.2	0.167	1.52	0.8	0.6?
$3s \ ^3P_2^o-3p \ ^3D_2$	5710.8	0.176	1.52	0.9	0.9
$3s \ ^3P_2^o-3p \ ^3D_1$	5730.7	0.167	0.10	–	–
$3s \ ^1P_1^o-3p \ ^3D_2$	5747.3	0.176	0.41	–	–
$3s \ ^1P_1^o-3p \ ^3D_1$	5767.5	0.167	0.19	–	–
$3p \ ^3P_0-3d \ ^3D_1^o$	5927.8	0.016	1.15	0.7?	1.0?
$3p \ ^3P_1-3d \ ^3D_2^o$	5931.8	0.035	1.72	1.4	2.0
$3p \ ^3P_1-3d \ ^3D_1^o$	5940.2	0.016	0.80	–	–
$3p \ ^3P_2-3d \ ^3D_3^o$	5941.7	0.096	2.05	1.2	1.5
$3p \ ^3P_2-3d \ ^3D_2^o$	5952.4	0.035	0.51	0.6?	1.2?
$3p \ ^3P_2-3d \ ^3D_1^o$	5960.9	0.016	0.05	–	–
$3s \ ^3P_1^o-3p \ ^1P_1$	6379.6	0.231	0.08	–	–
$3s \ ^1P_1^o-3p \ ^1P_1$	6482.0	0.231	0.38	–	–
$3d \ ^3P_2^o-4p \ ^3S_1$	6810.0	0.362	0.04	–	0.3?
$3d \ ^3P_1^o-4p \ ^3S_1$	6834.1	0.362	0.02	–	–
$3d \ ^3P_0^o-4p \ ^3S_1$	6847.2	0.362	0.01	–	–
$4s \ ^3P_2^o-4p \ ^3S_1$	14645.6	0.362	0.01	–	–

(1) Recombination contribution to total intensity.

(2) Predicted intensities with an $\text{H}\beta$ flux of $2.51 \text{ erg cm}^{-2} \text{ s}^{-1}$

(3) BVV

(4) EPG

which the LS coupling breaks down. The $3d \ ^5P$ term is autoionizing, and the most likely mechanism in this case is dielectronic recombination. EPG reported lines at $\lambda\lambda 6744.42$, 7535.32 and 9016.42 \AA that would be produced by highly excited d and f states of N^+ . Their identification as N II , however, is uncertain and their production in our model is very unlikely. Many more lines are predicted by our calcula-

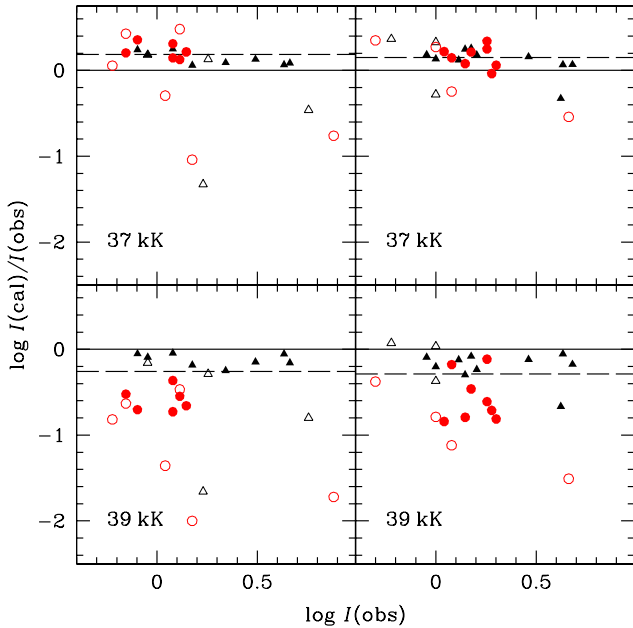


Figure 3. Comparison of intensities observed by BVV (left) and EPG (right panels) with predicted intensities of fluorescence lines from p states (triangles) and d states (circles) for two WMbasic stellar atmospheres. Open triangles and circles have uncertain I_{obs} (marked with “?” in table 5). The broken horizontal line is the value of $R = \langle I_{\text{cal}}/I_{\text{obs}} \rangle$. The nebular model was calculated with NEBU with BM parameters, except for $T_{\text{eff}} = 39$ kK in the lower panels, giving column densities of $N(\text{N}^+) = 7.3 \times 10^{16} \text{ cm}^{-2}$ and $2.6 \times 10^{16} \text{ cm}^{-2}$ for the $T_{\text{eff}} = 37$ kK and 39 kK atmospheres respectively. Note that the observed intensities here and in table 5 are normalized to $I(\text{H}\beta) = 10^4$.

tions, but their intensities are lower than the weaker lines reported by BVV or EPG, and their intensities are dominated by recombination. Intensities for other lines up to $n = 8$ and $l = 1$ are available from the authors upon request. Most of the observed lines with confident measurements fall within 0.2 dex of the predicted values in the basic model as shown in the upper panels of Fig. 3.

5 VARIATION OF PARAMETERS

5.1 Stellar temperature

Fig. 3 shows a comparison of observed and predicted intensities with two WMbasic atmospheres. The reduction in N^+ column density produced by the hotter star reduces the predicted intensities in general, but the intensities of the lines originating from d states suffer a much greater reduction than the ones from p states by an order of magnitude. We have traced this effect to an important decrease in the model atmosphere flux by a factor of ~ 2 at 529.6 \AA and a factor of ~ 5 at 533.7 \AA for $T_{\text{eff}} \gtrsim 38$ kK as shown in Fig. 4. As mentioned in section 2.1, 3d states are pumped almost entirely by absorptions at those two wavelengths. At the same time there is an increase of a factor of ~ 2 in the flux at 508.7 \AA for $T_{\text{eff}} \gtrsim 37$ kK, which is important in the pumping of 3p states, and compensates the decrease in the N^+ column density.

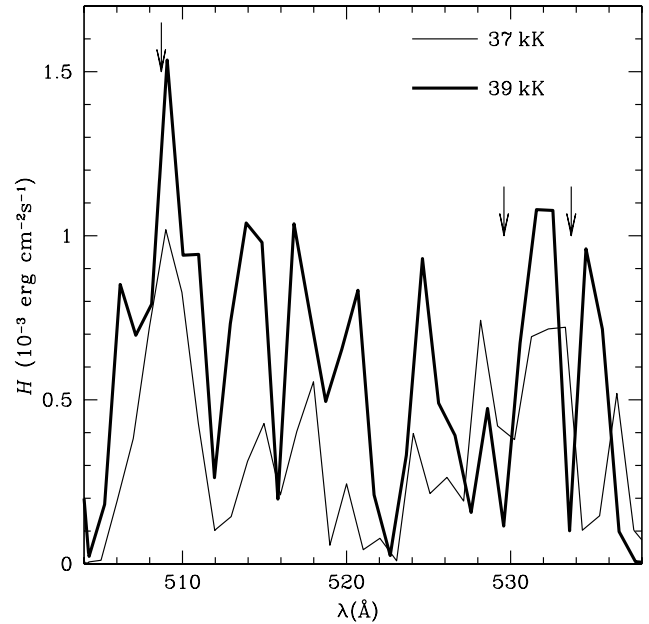


Figure 4. Surface Eddington flux of two WMbasic atmospheres. Arrows show wavelengths of the resonant multiplets at 508.7, 529.6 and 533.7 \AA .

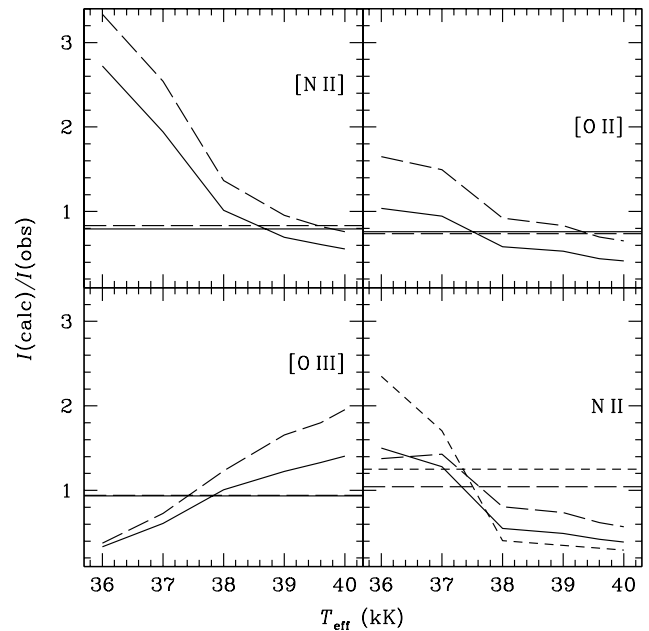


Figure 5. Intensities of some nebular diagnostic and N II permitted lines normalized to the observed values by BVV as a function of stellar T_{eff} . Top left: [NII] 6584 (solid), [NII] 5755 (dashed). Top right: [OII] 3729 (solid), [OII] 3726 (dashed). Bottom left: [OIII] 5007 (solid), [OIII] 4363 (dashed). Bottom right: N II permitted lines averaged $R = \langle I_{\text{cal}}/I_{\text{obs}} \rangle$ (solid), $\lambda 5941.65 \text{ \AA}$ (d upper state, short dash) and 4630.54 \AA (p upper state, long dash). Horizontal lines are the values observed by EPG. The nebular model was calculated with CLOUDY with the BM parameters, except for a varying T_{eff} .

The difference in the pumping rates of d and p states for $T_{\text{eff}} \gtrsim 38$ kK depends only on the shape of the spectrum and the contribution of recombination to the population of those states. Thus the disagreement between predicted and observed intensities of lines from d states with $T_{\text{eff}} = 39$ kK shown in Fig. 3 persists when the N abundance is increased to 1×10^{-4} or when the recombination contribution to the intensities is increased with the hypothesis of ultracold plasma proposed by Tsamis et al. (2004). A plasma temperature of 2000 K doubles the predicted intensities of lines from 3p states, but lines from 3d states increase their intensities in lower proportions because fluorescence is more important in the population of those states.

The other critical parameter in the fluorescence line intensities is the column density. The N^+ column density decreases with T_{eff} at a much lower rate for $T_{\text{eff}} \gtrsim 38$ kK as reflected in Fig. 5. The N II fluorescence lines and the [N II] lines decrease little for harder spectra due to that persistent N^+ concentration, but their different behaviour at lower T_{eff} can be understood in terms of the N^+ concentration and the escape probability concept. As shown in Fig. 2, the fluorescence N II lines form 50% of their intensity in the inner layers of the nebula, much closer to the star than the [N II] lines, which are produced in the outer N^+ zone. As T_{eff} decreases, the N^+ concentration and the optical depth of the resonant transitions increase, but the intensities of lines from p and d states behave differently as shown in Fig. 5 for the lines $3s \ ^3P_2 - 3p \ ^3P_2 \lambda 4630.54$ and $3p \ ^3P_2 - 3d \ ^3D_3 \lambda 5941.65$. Absorption transitions that populate the p states have a much lower optical depth than the ones pumping the d states. As a result the escape probability decreases more for d states than for p states with lower T_{eff} , and the pumping due to reabsorption of resonant photons for d states increases.

NEBU tends to give larger column densities than CLOUDY, and thus predicts higher intensities. Predicted line intensities by NEBU in the UV tend to be 30% more intense than those given by CLOUDY because NEBU does not consider internal dust extinction, but predictions of the two codes are within 20% of each other in the optical.

5.2 Kurucz atmospheres

CLOUDY contains a grid of low-resolution Kurucz atmospheres (Kurucz 1991) that can be readily used as continua in our calculations. A comparison of Fig. 3 and 6 shows that the differences between the calculated intensities of p and d states with Kurucz atmospheres are much smaller than the differences with the WMbasic atmospheres because the Kurucz atmospheres do not have the structure of the WMbasic atmospheres that causes the different absorption rates between p and d states.

Modeling of Orion with CLOUDY (Baldwin et al. 1991, 1996, 2000) has favored stellar temperatures that are lower than current spectro-photometric measurements. Our results with the WMbasic atmospheres also favor a lower T_{eff} , but Kurucz atmospheres give a better agreement with observations because they are softer than other models and give a larger N^+ column.

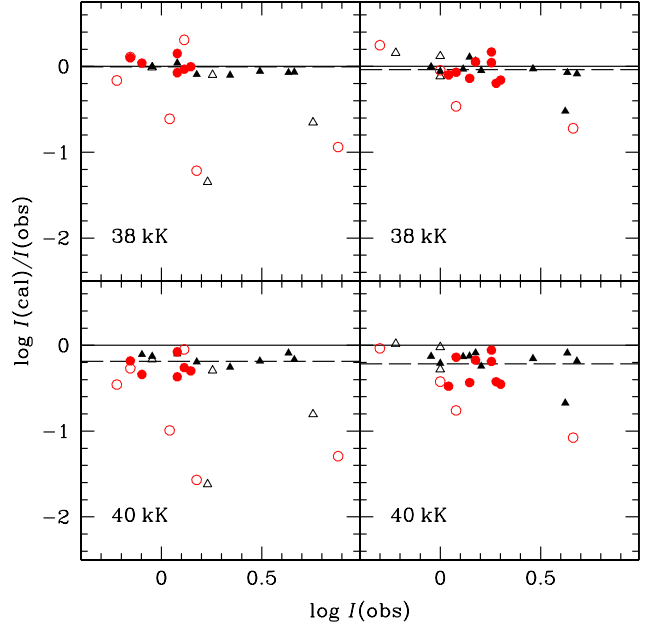


Figure 6. Same as Fig. 3, but for two Kurucz atmospheres. The N^+ column densities are $N(N^+) = 3.5 \times 10^{16} \text{ cm}^{-2}$ and $1.13 \times 10^{16} \text{ cm}^{-2}$ for the $T_{\text{eff}} = 38$ kK and 40 kK atmospheres respectively.

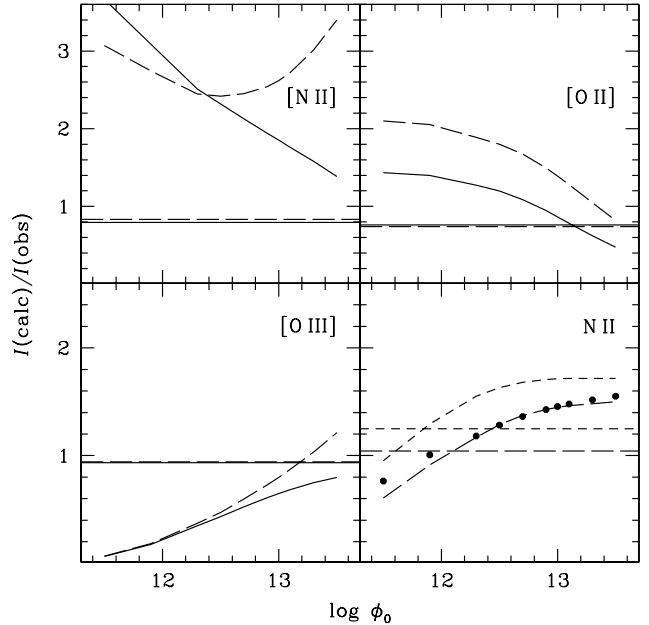


Figure 7. Same as Fig. 5, but with $T_{\text{eff}} = 37$ kK and varying ϕ_0 . The average $R = I_{\text{cal}}/I_{\text{obs}}$ (not shown) is within 3% of the 4630.54 Å line. The fit of equation (11) (dots) is normalized to the 4630.54 Å line at $\log \phi_0 = 12.9$.

5.3 Stellar flux

Unlike most forbidden and recombination lines, fluorescence line intensities are more sensitive to changes in the stellar flux illuminating the nebula. Their intensities increase with ϕ_0 up to $10^{12.5} \text{ cm}^{-2} \text{ s}^{-1}$ and remain nearly constant for higher ϕ_0 . This behavior can be understood in similar terms to the curve of growth of the resonant lines. As the intensity of the ionizing flux grows, the N^+ column density and the optical depth increase, and the cores of the resonant lines become saturated. Eqs. 2 and 9 show that the intensity of the fluorescence lines is approximately proportional to the integral along the line of sight of the pumping rate of equation (2) times the density of the absorbing state, $n_g \beta_{gj}$. Changing variable from r to τ_0 , eliminating constant quantities and assuming a constant Doppler width, the intensity of a fluorescence line will be

$$I \propto \int_0^\infty \bar{J}_\nu \int e^{-\tau_0 \phi(x)} \phi(x) dx d\tau_0 \\ = J_\nu(0) \int_0^\infty e^{-\tau_c} \int e^{-\tau_0 \phi(x)} \phi(x) dx d\tau_0 .$$

where $J_\nu(0)$ is the stellar continuum at the illuminated face of the cloud, and τ_c is the continuum opacity. The integration over τ_0 can be performed exactly if we assume a mean value for $e^{-\tau_c}$. For fixed T_{eff} and ν , $J_\nu(0)$ is proportional to ϕ_0 , which in turn is proportional to the $\text{H}\beta$ flux. Therefore the fluorescence line intensity normalized to $\text{H}\beta$ must be proportional to

$$\langle e^{-\tau_c} \rangle \int (1 - e^{-\tau_0 \phi(x)}) dx .$$

The integral is proportional to the curve of growth $W(\tau_0)$. Fig. 7 shows that the intensity of the lines follows closely a fit of the form

$$I/I(\text{H}\beta) \propto e^{-2.5 \times 10^{-22} N(\text{H}^+)} W(\tau_0) . \quad (11)$$

where $N(\text{H}^+)$ is the H^+ column density in cm^{-2} and $W(\tau_0)$ is the curve of growth of the $2p^2 \text{ } ^3\text{P}_2 - 4s \text{ } ^3\text{P}_2^o \lambda 508.697 \text{ \AA}$ line, which pumps most of the 4630.54 line.

6 CONCLUSIONS

The intensity of the lines in the N II spectrum of the Orion nebula can be explained by fluorescence of the UV radiation of $\theta^1 \text{ C Ori}$ in the ionized gas. Recombination of N^{+2} contributes a minor part of the observed intensities of lines from 3p and 3d levels connected to the ground state. The effective temperature of the star must be below 38000 K in order to reproduce the observed line intensities with typical ionization models that are consistent with the forbidden line intensities. An increased N abundance does not allow the use of a higher star temperature. The existence of intervening ionized material in the foreground (O'Dell et al. 1993) was not considered in our model and may help increase the predicted intensities of the N II lines. Fluorescence does not increase the intensity of the lines from 4f levels, and other mechanisms must be proposed to explain their strong intensities with respect to the collisionally excited and fluorescence lines in the Orion nebula.

ACKNOWLEDGMENTS

The authors are very grateful to Katia Verner and Gary Ferland for valuable advice in running CLOUDY.

REFERENCES

- Afflerbach A., Churchwell E., Werner M. W., 1997, ApJ, 478, 190
- Allen C. W., 1973, “Astrophysical Quantities”, 3rd ed., §27, The Athlone Press, London.
- Baldwin J. A., Ferland G. J., Martin P. G., Corbin, M. R., Cota S. A., Peterson B. M., Slettebak A., 1991, ApJ, 374, 580
- Baldwin J. A., Crots A., Dufour R. J., Ferland G. J., Heathcote S., Hester J. J., Korista K. T., Martin P. G., O'Dell C. R., Rubin R. H., Tielens A. G. G. M. Verner, D. A., Verner E. M., Walter, D. K., Wen Z., 1996, ApJ Letters, 468, L115
- Baldwin J. A., Verner E. M., Verner D. A; Ferland G. J., Martin P. G., Korista K. T. & Rubin R. H., 2000, ApJS, 129, 229 (BVV)
- Balick B.; Gammon R. H.; Hjellming R. M., 1974, PASP, 86, 616
- Bell K. L., Hibbert A., Stafford R. P., 1995, Physica Scripta, 52, 251
- Cowan R. D., Andrew K. C., 1965, J. of the Optical Society of America, 55, 502
- Cunha K., Lambert D. L., 1994, ApJ, 426, 170
- Dumont A.-M., Collin S., Paletou F., Coupé S., Godet O., Pelat D., 2003, A&A, 407, 13
- Escalante V., 2002, RevMexAA (Serie de Conferencias), 12, 22
- Escalante V., Góngora-T. A., 1990, ApJS, 74, 819
- Escalante V., Victor G. A., 1990, ApJS, 73, 513 (EV)
- Esteban C., Peimbert M., Torres-Peimbert S., Escalante V., 1998, MNRAS, 295, 401
- Esteban C., Peimbert M., García-Rojas J., Ruiz M. T., Peimbert A., Rodríguez M., 2004, MNRAS, to be published (EPG)
- Ferland G. J., 1992, ApJ Letters, 389, L63
- Ferland G. J., 1996, Hazy, a Brief Introduction to CLOUDY, University of Kentucky Department of Physics and Astronomy Internal Report.
- Ferland G. J., 2001, PASP, 113, 41
- Grandi S. A., 1976, ApJ, 206, 658
- Hillenbrand L. A., 1997, AJ, 113, 1733
- Howarth I. D., Prinja R. K., 1989, ApJS, 69, 527
- Hummer D. G., 1968, MNRAS, 138, 73
- Hummer, D. G., Storey, P. J., 1992, MNRAS, 254, 277
- Kisielius R., Storey P. J., 2002, A&A, 387, 1135
- Kurucz R. L., 1991, in Proc. of the Workshop on Precision Photometry: Astrophysics of the Galaxy, ed. A. C. Davis Philips, A. R. Uppgren K. A. James (Schenectady, NY: Davis), p. 27
- Liu X.-W., Storey P. J., Barlow M. J., Clegg R. E. S., 1995, MNRAS, 272, 369
- Liu X.-W., Storey P. J., Barlow M. J., Danziger, I. J., Cohen, M., Bryce, M., 2000, MNRAS, 312, 585
- Liu X.-W., Luo S.-G., Barlow M. J., Danziger I. J., Storey P. J., 2001, MNRAS, 327, 141

- Luo S.-G., Liu X.-W., Barlow M. J., 2001, MNRAS, 326, 1049
- Morisset C., Schaerer D., Martín-Hernández N. L., Peeters E., Damour F., Baluteau J.-P., Cox P., Roelfsema P., 2002, A&A, 386, 558
- Murphy T., Meiksin A., 2004, to appear in MNRAS, astro-ph/0404010.
- Nussbaumer H., Storey P. J., 1984, A&A Suppl., 56, 293
- O'Dell C. R., Valk J. H., Wen Z., Meyer D. M., 1993, ApJ, 403, 678
- Pauldrach A. W. A., Hoffmann T. L., Lennon M., 2001, A&A, 375, 161
- Peimbert M., Peimbert A., Ruiz M. T., Esteban C., 2004, ApJS, 150, 431
- Péquignot D., Petitjean P., Boisson C., 1991, A&A, 251, 680
- Péquignot D., et al., 2001, in Ferland G. J., Savin D. W., eds., ASP Conf. Ser. Vol. 247, Spectroscopic Challenges of Photoionized Plasmas, Astron. Soci. Pac., San Francisco, p. 1
- Shaver P. A., McGee R. X., Newton L. M., Danks A. C., Pottasch S. R., 1983, MNRAS, 204, 53
- Seaton M. J. 1959, MNRAS, 119, 70
- Seaton M. J. 1968, MNRAS, 139, 129
- Seaton M. J., Yu Yan, Mihalas D., Pradhan A. K., 1994, MNRAS, 266, 805
- Sharpee B., Williams R., Baldwin J. A., van Hoof, P. A. M., 2003, ApJS, 149, 157
- Smith L. J., Norris R. P. F., Crowther P. A., 2002, MNRAS, 337, 1309
- Stasińska G., Schaerer D., 1997, A&A, 322, 615
- Sternberg A., Hoffmann T. L., Pauldrach A. W. A., 2003, ApJ, 599, 1333
- Tsamis Y. G., Barlow M. J., Liu X.-W., Danziger I. J., Storey P. J., 2003, MNRAS, 345, 186
- Tsamis Y. G., Barlow M. J., Liu X.-W., Storey P. J., Danziger I. J., 2004, MNRAS, 353, 953
- Victor G. A., Escalante V., 1988, Atomic Data and Nuclear Data Tables, 40, 227
- Wen Z., O'Dell C. R., 1995, ApJ, 438, 784
- Wiese W. L., Fuhr J. R., Deters T. M., 1996, Atomic Transition Probabilities of Carbon, Nitrogen, and Oxygen, Journal of Physical Chemical Reference Data Monograph No. 7, American Chemical Society, New York, p. 194
- Zuckerman B., 1973, ApJ, 183, 863